Biomedical Optics EXPRESS

Dual-channel spectrally encoded endoscopic probe

Guy Engel,[1] Hadar Genish,[2] Michael Rosenbluh,[2] and Dvir Yelin[1,*]

[1]*Department of Biomedical Engineering, Technion—Israel Institute of Technology, Haifa 32000, Israel*
[2]*Department of Physics, Faculty of Exact Sciences, Bar-Ilan University, Ramat-Gan 52900, Israel*
**yelin@bm.technion.ac.il*

Abstract: High quality imaging through sub-millimeter endoscopic probes provides clinicians with valuable diagnostics capabilities in hard to reach locations within the body. Spectrally encoded endoscopy (SEE) has been shown promising for such task; however, challenging probe fabrication and high speckle noise had prevented its testing in *in vivo* studies. Here we demonstrate a novel miniature SEE probe which incorporates some of the recent progress in spectrally encoded technology into a compact and robust endoscopic system. A high-quality miniature diffraction grating was fabricated using automated femtosecond laser cutting from a large bulk grating. Using one spectrally encoded channel for imaging and a separate channel for incoherent illumination, the new system has large depth of field, negligible back reflections and well controlled speckle noise which depends on the core diameter of the illumination fiber. Moreover, by using a larger imaging channel, higher groove density grating, shorter wavelength and broader spectrum, the new endoscopic system now allow significant improvements in almost all imaging parameter compared to previous systems, through an ultra-miniature endoscopic probe.

OCIS codes: (110.2350) Fiber optics imaging; (170.0170) Medical optics and biotechnology; (170.2150) Endoscopic imaging; (220.4610) Optical fabrication; (330.1710) Color, measurement.

References and links

1. T. Nakamura and A. Terano, "Capsule endoscopy: past, present, and future," J. Gastroenterol. **43**(2), 93–99 (2008).
2. Z. Fireman, E. Mahajna, E. Broide, M. Shapiro, L. Fich, A. Sternberg, Y. Kopelman, and E. Scapa, "Diagnosing small bowel Crohn's disease with wireless capsule endoscopy," Gut **52**(3), 390–392 (2003).
3. M. V. Sivak, Jr. and D. E. Fleischer, "Colonoscopy with a VideoEndoscope: preliminary experience," Gastrointest. Endosc. **30**(1), 1–5 (1984).
4. A. F. Gmitro and D. Aziz, "Confocal microscopy through a fiber-optic imaging bundle," Opt. Lett. **18**(8), 565–567 (1993).
5. R. T. Kester, T. Christenson, R. R. Kortum, and T. S. Tkaczyk, "Low cost, high performance, self-aligning miniature optical systems," Appl. Opt. **48**(18), 3375–3384 (2009).
6. B. I. Hirschowitz, "Endoscopic examination of the stomach and duodenal cap with the fiberscope," Lancet **278**(7186), 1074–1078 (1961).
7. F. Ishibashi, K. Aziz, G. S. Abela, and S. Waxman, "Update on coronary angioscopy: review of a 20-year experience and potential application for detection of vulnerable plaque," J. Interv. Cardiol. **19**(1), 17–25 (2006).
8. D. C. Zavala, "Diagnostic fiberoptic bronchoscopy: Techniques and results of biopsy in 600 patients," Chest **68**(1), 12–19 (1975).
9. H. D. Jho, R. L. Carrau, Y. Ko, and M. A. Daly, "Endoscopic pituitary surgery: an early experience," Surg. Neurol. **47**(3), 213–222, discussion 222–223 (1997).
10. T. Matsunaga, Y. Kawakami, K. Namba, and M. Fujii, "Intraductal biopsy for diagnosis and treatment of intraductal lesions of the breast," Cancer **101**(10), 2164–2169 (2004).
11. V. R. Jacobs, M. Kiechle, B. Plattner, T. Fischer, and S. Paepke, "Breast ductoscopy with a 0.55-mm mini-endoscope for direct visualization of intraductal lesions," J. Minim. Invasive Gynecol. **12**(4), 359–364 (2005).
12. D. L. Dickensheets and G. S. Kino, "Micromachined scanning confocal optical microscope," Opt. Lett. **21**(10), 764–766 (1996).
13. A. L. Polglase, W. J. McLaren, S. A. Skinner, R. Kiesslich, M. F. Neurath, and P. M. Delaney, "A fluorescence confocal endomicroscope for in vivo microscopy of the upper- and the lower-GI tract," Gastrointest. Endosc. **62**(5), 686–695 (2005).

#166904 - $15.00 USD Received 18 Apr 2012; revised 2 Jul 2012; accepted 2 Jul 2012; published 16 Jul 2012

14. W. Drexler and J. G. Fujimoto, *Optical Coherence Tomography: Technology and Applications* (Springer, 2008).
15. G. J. Tearney, M. E. Brezinski, B. E. Bouma, S. A. Boppart, C. Pitris, J. F. Southern, and J. G. Fujimoto, "In vivo endoscopic optical biopsy with optical coherence tomography," Science **276**(5321), 2037–2039 (1997).
16. E. J. Seibel and Q. Y. J. Smithwick, "Unique features of optical scanning, single fiber endoscopy," Lasers Surg. Med. **30**(3), 177–183 (2002).
17. G. J. Tearney, M. Shishkov, and B. E. Bouma, "Spectrally encoded miniature endoscopy," Opt. Lett. **27**(6), 412–414 (2002).
18. D. Yelin, I. Rizvi, W. M. White, J. T. Motz, T. Hasan, B. E. Bouma, and G. J. Tearney, "Three-dimensional miniature endoscopy," Nature **443**(7113), 765 (2006).
19. D. Yelin, B. E. Bouma, and G. J. Tearney, "Volumetric sub-surface imaging using spectrally encoded endoscopy," Opt. Express **16**(3), 1748–1757 (2008).
20. D. Yelin, B. E. Bouma, J. J. Rosowsky, and G. J. Tearney, "Doppler imaging using spectrally-encoded endoscopy," Opt. Express **16**(19), 14836–14844 (2008).
21. D. Kang, D. Yelin, B. E. Bouma, and G. J. Tearney, "Spectrally-encoded color imaging," Opt. Express **17**(17), 15239–15247 (2009).
22. D. Yelin, W. M. White, J. T. Motz, S. H. Yun, B. E. Bouma, and G. J. Tearney, "Spectral-domain spectrally-encoded endoscopy," Opt. Express **15**(5), 2432–2444 (2007).
23. D. Yelin, B. E. Bouma, S. H. Yun, and G. J. Tearney, "Double-clad fiber for endoscopy," Opt. Lett. **29**(20), 2408–2410 (2004).
24. S. Lemire-Renaud, M. Rivard, M. Strupler, D. Morneau, F. Verpillat, X. Daxhelet, N. Godbout, and C. Boudoux, "Double-clad fiber coupler for endoscopy," Opt. Express **18**(10), 9755–9764 (2010).
25. A. Abramov, L. Minai, and D. Yelin, "Spectrally encoded spectral imaging," Opt. Express **19**(7), 6913–6922 (2011).
26. C. Pitris, B. E. Bouma, M. Shiskov, and G. J. Tearney, "A GRISM-based probe for spectrally encoded confocal microscopy," Opt. Express **11**(2), 120–124 (2003).
27. D. Yelin, C. Boudoux, B. E. Bouma, and G. J. Tearney, "Large area confocal microscopy," Opt. Lett. **32**(9), 1102–1104 (2007).
28. D. Kang, M. J. Suter, C. Boudoux, H. Yoo, P. S. Yachimski, W. P. Puricelli, N. S. Nishioka, M. Mino-Kenudson, G. Y. Lauwers, B. E. Bouma, and G. J. Tearney, "Comprehensive imaging of gastroesophageal biopsy samples by spectrally encoded confocal microscopy," Gastrointest. Endosc. **71**(1), 35–43 (2010).
29. C. Boudoux, S. C. Leuin, W. Y. Oh, M. J. Suter, A. E. Desjardins, B. J. Vakoc, B. E. Bouma, C. J. Hartnick, and G. J. Tearney, "Preliminary evaluation of noninvasive microscopic imaging techniques for the study of vocal fold development," J. Voice **23**(3), 269–276 (2009).
30. M. D. Perry, B. C. Stuart, P. S. Banks, M. D. Feit, V. Yanovsky, and A. M. Rubenchik, "Ultrashort-pulse laser machining of dielectric materials," J. Appl. Phys. **85**(9), 6803–6810 (1999).
31. J. W. Goodman, "Some fundamental properties of speckle," J. Opt. Soc. Am. **66**(11), 1145–1150 (1976).
32. J. W. Goodman and E. G. Rawson, "Statistics of modal noise in fibers: a case of constrained speckle," Opt. Lett. **6**(7), 324–326 (1981).
33. H. S. Fairman, M. H. Brill, and H. Hemmendinger, "How the CIE 1931 color-matching functions were derived from Wright-Guild data," Color Res. Appl. **22**(1), 11–23 (1997).
34. J. Y. Hardeberg, *Acquisition and Reproduction of Color Images: Colorimetric and Multispectral Approaches* (Dissertation.com, 2001).
35. A. Abramov, L. Minai, and D. Yelin, "Multiple-channel spectrally encoded imaging," Opt. Express **18**(14), 14745–14751 (2010).

1. Introduction

With the recent advance in fiber optics and digital imaging technologies, minimally invasive, miniature endoscopes have begun to find widespread applications in numerous clinical disciplines. Miniature cameras are currently used mainly for imaging within the GI system [1–3], while fiber-bundle endoscopes [4,5] are currently studied or used for various applications in the upper GI tract [6], cardiovascular system [7], lungs [8], ENT [9], mammary ducts [10,11], and other difficult to reach areas. Distal mirror scanning has also been proposed [12] and demonstrated [13] to be useful for imaging in the upper and lower GI tract. Other promising technologies for miniature endoscopy which use only a single optical fiber include optical coherence tomography [14,15] and resonant fiber scanning [16]; both techniques are currently at advance stages of clinical study and validation.

In the past decade, a technique termed spectrally encoded endoscopy (SEE) [17] has been shown to be promising for single fiber endoscopic imaging with a high number of resolvable points. The wide range of capabilities of SEE was demonstrated mainly on the optical bench, and includes three-dimensional imaging at video-rates [18], subsurface imaging [19], Doppler imaging [20], as well as color [21] and spectral [21] imaging. In parallel to demonstrating these capabilities, an ultra-miniature endoscopic SEE probe with 350 μm diameter has been described [22] and demonstrated by imaging the parietal peritoneal wall of a mouse model, *in*

#166904 - $15.00 USD Received 18 Apr 2012; revised 2 Jul 2012; accepted 2 Jul 2012; published 16 Jul 2012

vivo [18]. In order to resolve three dimensional tissue structures with high signal-to-noise ratio (SNR), low coherence interferometry between the reflected encoded light and a reference signal has been utilized within a fiber optic Michelson interferometer. Such a configuration had the additional benefit of overcoming back reflections from various interfaces within the miniature probe. Yet, such an interferometric SEE system has several limitations, including pronounced speckle noise due to the high spatial coherence of the single-mode fiber, short depth of field due to the confocal gating and limited spectrometer resolution, and necessitates a relatively complex alignment of the optical interferometer.

Separating the illumination from the collection optical paths using a dual-clad fiber has allowed [23] low speckle imaging with a large depth of field and high signal throughput. A miniature SEE probe with a dual-clad fiber, however, had suffered from background signal from reflections within the probe optics; such high background resulted in overwhelming shot noise and difficulty at subtracting the time-varying reflections during the constant probe motion (unpublished data). Using a dedicated dual-clad fiber coupler [24] could potentially improve the performance of a future dual-clad probe by eliminating reflections from the proximal fiber end; such coupler, however, could not effectively remove reflections from the distal probe optics.

In this work, we present a novel SEE probe which uses two separated illumination and imaging channels for obtaining background-free non-interferometric endoscopic imaging. By using two individual fibers: a large multimode core fiber for illumination and a single-mode fiber for imaging, we demonstrate effective imaging with a large number of resolvable points, low speckle contrast and a large depth of field. For improving image quality, we develop a technique for laser-cutting high quality miniature gratings from a large bulk grating, and study the dependence of speckle contrast on the illumination fiber core diameter. Finally, we demonstrate color imaging by optimizing the probe's optics for the visible wavelength and utilizing two-dimensional lateral scanning [25].

2. Methods and experimental setup

2.1. Probe construction

Due to its complex structure, the miniature diffraction grating at the distal end of a SEE probe is the most challenging component to manufacture. Previous experimental demonstrations of spectrally encoded imaging probes have utilized either 10 mm diameter grating within a prism-GRISM configuration [26] or approximately 7 mm x 10 mm rectangular gratings [27–29]. A sub-millimeter diameter SEE probe has been also demonstrated [18,22] utilizing a 350 μm diameter transmission grating which was fabricated by imprinting a linear grating pattern on an epoxy resin (Holographix LLC) at the angled tip of a large core fiber. A main limitation of such fabrication process was its high complexity and high manufacturing cost of separating the miniature gratings from their aluminum and epoxy fixtures. Other difficulties included the preparation of a large number of angle-polished glass rods within a uniform substrate and achieving high optical uniformity across the imprinted surfaces.

We have developed a new technique for producing miniature gratings by cutting out arbitrary shaped pieces from a large, high efficiency transmission grating, using a tightly focused femtosecond laser beam. A 0.65-mm-thick, 20 mm x 20 mm square fused silica grating (FSTG-VIS-1379-902, 1379 lines/mm, 550 nm maximum efficiency wavelength, Ibsen photonics) was mounted on a computer controlled x-y-z translation stage (3 × M-122.2DD, Physik Instrumente, GmbH) and was cut by a high irradiance pulse beam (45 fs pulse duration, 800 nm central wavelength, 1 kHz repetition rate, Spitfire-Pro XP, Newport Corp.) which was focused by a 0.62 NA aspheric lens onto the grating glass (Fig. 1(a)). The angle between the grating normal and the beam optical axis was set equal to the Littrow's angle (17.9°) of the central 550 nm imaging wavelength, potentially allowing the extraction of more than four hundred slanted, 500-μm-diameter cylindrical gratings. After cutting, each individual piece was cleaned in an ultrasonic acetone bath and then polished for obtaining a flat bottom surface perpendicular to the optical axis. Due to the ultrashort pulses and low

#166904 - $15.00 USD Received 18 Apr 2012; revised 2 Jul 2012; accepted 2 Jul 2012; published 16 Jul 2012

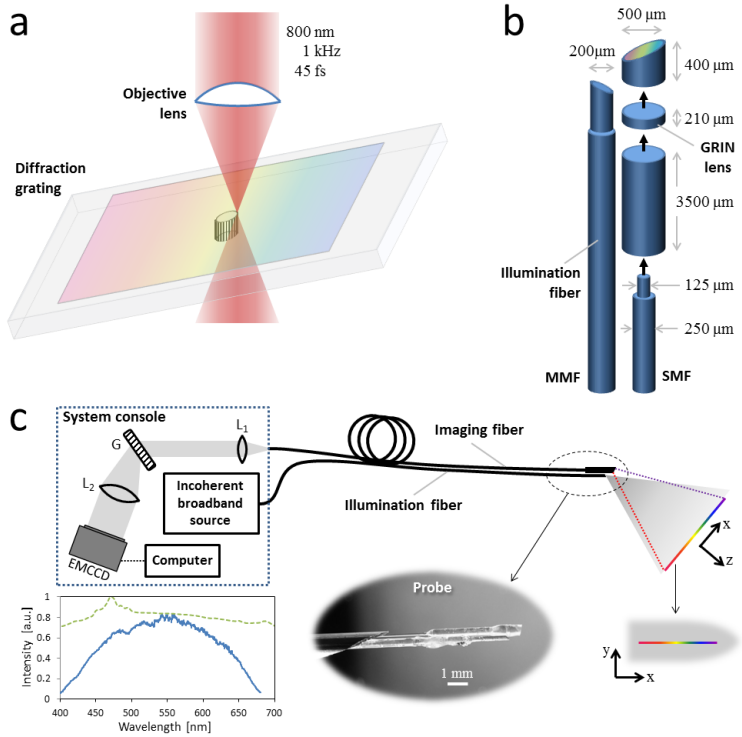

Fig. 1. (a) Cutting of a miniature diffraction grating from a large silica transmission grating using focused intense Ti:sapphire pulses. (b) Dual-channel SEE probe assembly. SMF—single-mode fiber. MMF—multi-mode fiber. (c) Schematic drawing of the dual-channel SEE system. Bottom-left inset—measured spectrum from a white sample (blue curve) compared to the source spectrum (dashed green curve). Bottom-middle inset—a close-up photograph of the distal end of the dual-channel probe. Bottom-right inset—schematic of the relative positions of the illumination spot and the spectrally encoded imaged line. L1 and L2—achromatic lenses. G—diffraction grating. EMCCD—electron-multiplying charge coupled device.

repetition rates used [30], relatively small imperfections ("chip") of up to 40 µm in size were present at the grating edges. Average diffraction efficiency (1st order power divided by total transmitted power) of four measured 500-µm-diameter gratings was approximately 75.7%, somewhat lower than the intact grating efficiency of 89.6%, probably due to residual glass dust which remained on the grating surface.

Assembly of the imaging channel was accomplished (Fig. 1(b)) by gluing together the miniature grating, a 0.21-mm-long GRIN lens (ILW-050-WD05, NSG Europe), a 3.5-mm-long 400-µm-diameter spacer, and the distal end of a single-mode fiber (S460HP, Nufern). The working distance was approximately 10 mm (measured from the distal grating surface to the focal plane). Similar assembly procedure of an imaging spectrally encoded probe was described in Ref [22]. The illumination channel of the probe was comprised (Fig. 1(b)) of a large diameter core fiber whose distal end was stripped from its coating and placed adjacent to the imaging probe. For matching the imaging angle (35.8°, twice the Littrow's angle for the center wavelength), the distal illumination fiber end was polished at an angle of approximately 40°, resulting in an illumination at an angle around 33.6° with respect to the probe's optical axis (Fig. 1(c)). Four different illumination fibers were tested in this work, having core diameters of 100 µm (NA = 0.22), 200 µm (NA = 0.22), 400 µm (NA = 0.37) and 600 µm (NA = 0.37). Both the illumination and imaging channels were inserted into a 1.2 mm outer diameter stainless-steel needle which was mounted on an optical table for testing its imaging performance.

#166904 - $15.00 USD Received 18 Apr 2012; revised 2 Jul 2012; accepted 2 Jul 2012; published 16 Jul 2012

2.2. Experimental setup

Incoherent broadband light from a high brightness laser-driven light source (LDLS) (EQ-99FC, Energetiq Technology) was coupled into the 200 cm-long multimode illumination fiber, resulting in an illumination spot with a characteristic elliptical shape on the sample. The relatively large angle (40°) of the distal end of the fiber resulted in a sharp-cropped edge due to total internal reflection within the fiber. For the two numerical apertures of 0.22 and 0.37 of the tested fibers, the long axis of the illumination spot was approximately 7.5 mm and 10 mm, respectively, longer than the parallel 4.7-mm-long spectrally encoded line (Fig. 1(c), bottom-right inset).

Light collected by the spectrally encoded imaging channel was directed through the 2 m long single-mode fiber to the system console (dashed rectangle in Fig. 1(c)), collimated by an achromatic lens (Leica, Achro, 0.1 NA), diffracted by a 1379 lines/mm transmission grating (FSTG-VIS-1379-902, Ibsen photonics) and focused onto a high aspect ratio (200 x 1600 pixels) EMCCD array (DU970N-BV, Andor Technology plc.) using a 50 mm focal length lens (Nikon AFC) (Fig. 1(c)). The resolution of the spectrometer was approximately 0.44 nm, limited mainly by the pixel size of the EMCCD. A measured spectrum from a white card placed at the focal plane of the probe showed a total imaging bandwidth of 400–680 nm (Fig. 1(c), bottom-left inset, blue curve) which was used to encoded space at 14.5 nm/μm with spectral resolution of approximately 1 nm (limited by the probes optics). The illumination spectrum form the LDLS at that wavelength range is shown for reference (Fig. 1(c), bottom-left inset, dashed green curve). Alignment of the illumination and imaging channels within the probe was accomplished by adjusting the rotation angle of the illumination fiber for maximizing the resulting image intensity. A photograph of the distal end of the dual-channel SEE probe is shown in the bottom-middle inset of Fig. 1(c).

3. Results

3.1. Probe performance

In order to study the imaging characteristics of our dual-channel SEE probe, a 1951 USAF scattering resolution target (NT57-896, Edmund optics) was first imaged using a probe with a 200-μm-diameter core illumination fiber (Fig. 2(a)). The lateral (x-axis) field of view was approximately 4.7 mm, in good agreement with the predicted theoretical value of 4.05 mm. The lateral resolution at the center of the image was (edge response, FWHM) approximately 23 μm, 58% lower than the predicted values of 14.58 μm (assuming effective probe diameter of 460 μm), most likely due to imperfections in the probe's grating and the effect of speckle noise. The depth of field, i.e. twice the distance between the focal plane and the plane at which lateral resolution drops to one half of its highest value, was approximately 4.35 mm. Due to the non-confocal nature of the probe, the resolution target was still visible far beyond that range though, albeit with lower resolution.

To study the effect of the illumination core diameter on speckle noise, the resolution target was illuminated using probes with fibers having 100 μm, 200 μm, 400 μm and 600 μm diameter cores (Fig. 2(b)). Noticeably, speckle contrast was less prominent for larger core fibers, significantly improving the apparent resolution and image quality. Measuring the speckle contrast at regions of interest marked by white dotted rectangles (magnified at the bottom panels in Fig. 2(b)) have confirmed our visual impression, showing monotonic, nearly linear reduction of speckle contrast as illumination core diameter increases (Fig. 2(c)). The observed speckle noise reduction could be partially explained by correlating the speckle contrast with the number of propagation modes within the fiber, which result in uncorrelated speckled illumination patterns [31]. The square root dependence of the speckle contrast on the number of modes, which, in turn, depend quadratically on the core diameter, agrees well with the observed linear decrease in speckle contrast shown in Fig. 2(c). Exact calculation of the expected speckle contrast would require detailed knowledge of the relative illuminated and imaged areas [32], as well as quantitative understanding of the diffused scattering within the sample.

#166904 - $15.00 USD Received 18 Apr 2012; revised 2 Jul 2012; accepted 2 Jul 2012; published 16 Jul 2012

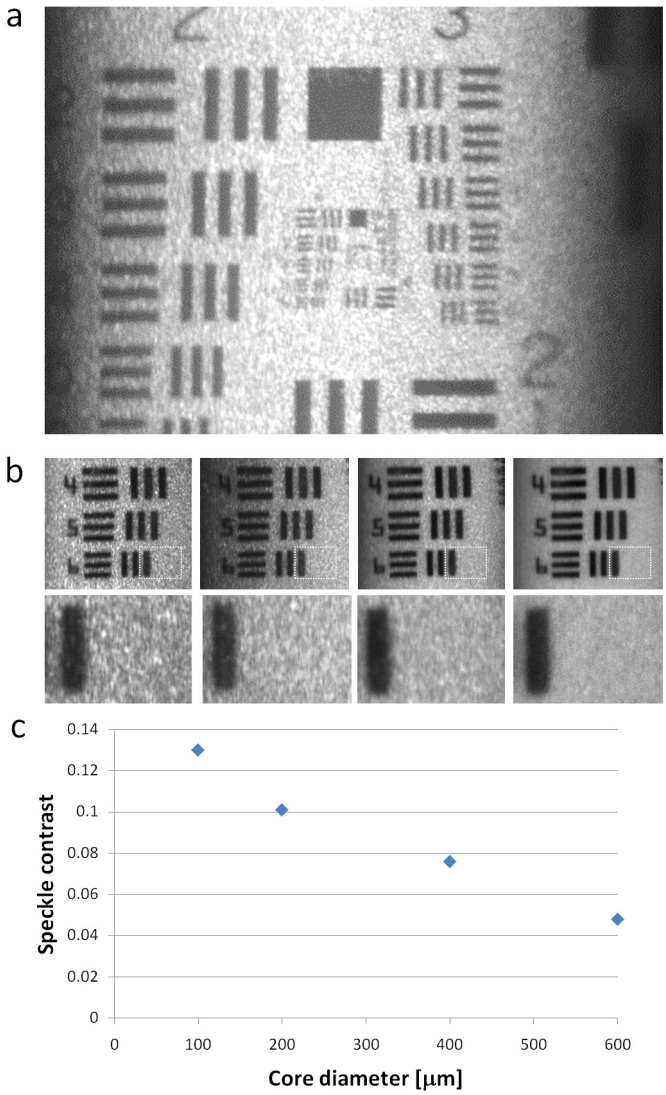

Fig. 2. (a) Image of a 1951 USAF scattering resolution target using a 200 μm diameter core illumination fiber. (b) Magnified views of region of interest using illumination fibers with varying core diameters. Higher magnification views of the corresponding regions marked by dashed rectangles are shown in the bottom panels. (c) Speckle contrast for different illumination core diameters.

In order to measure the SNR of the system for imaging tissue, a finger of a volunteer was imaged at 1 kHz line rate, which corresponds to 2 Hz frame (500 lines) rate. The nail plate and nail fold are clearly visible in the image (Fig. 3) which also shows fine details in the skin structure. The SNR at the uniform and relatively dark region of the nail was approximately 6.8 dB. Several important imaging parameters of the dual-channel SEE system and probe are summarized in Table 1 and compared to the expected theoretical values of an equivalent 460 μm diameter probe (considering the average 40 μm grating edge imperfections).

Compared to the previously demonstrated interferometric SEE system with a single fiber probe [18,22], the lateral resolution of the current dual-channel system and probe has improved by 23% (from 30 μm to 23 μm), field of view has increased by 80% from 2.6 mm to 4.7 mm, depth of field has improved by 46% from 2.97 mm to 4.35 mm, the number of resolvable points has increased by 70% from 120 to 204 (or by a factor of three for a square

#166904 - $15.00 USD Received 18 Apr 2012; revised 2 Jul 2012; accepted 2 Jul 2012; published 16 Jul 2012

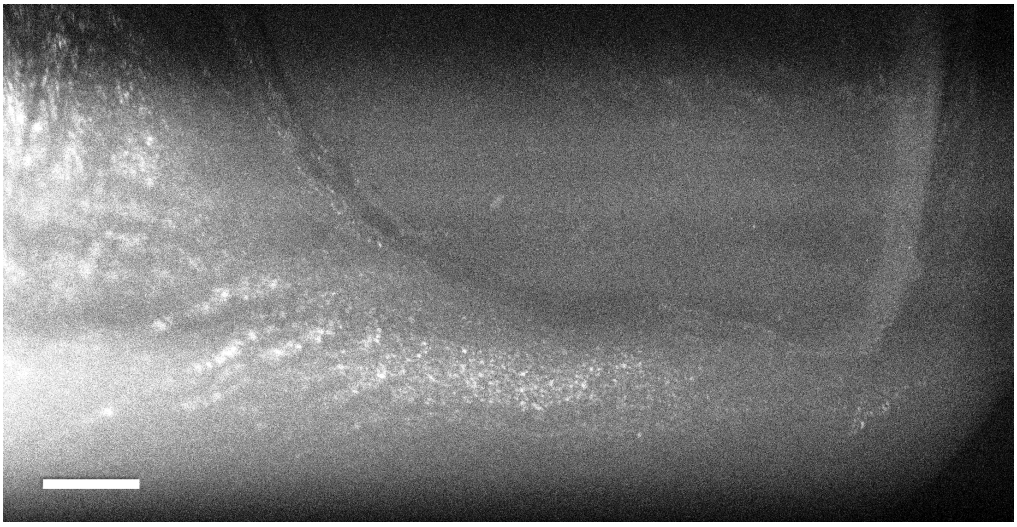

Fig. 3. Imaging of a volunteer's finger at 1 kHz line rate. Scale bar represents 1 mm.

Table 1. Imaging parameters of the SEE system and probe

	Measured	Theoretical
Lateral resolution	23 μm	14.58 μm
Field of view (x axis)	4.7 mm	4.05 mm
Number of resolvable points (x axis)	204	278
Depth of focus	4.35 mm	1.05 mm
SNR (nail, 1 kHz line rate)	6.8 dB	–
Speckle contrast (200 μm illumination fiber)	0.1	–

image), and speckle contrast has improved by 7.6-fold from approximately 0.76 [23] down to 0.1. On the down side, imaging line rate has decreased from 6 kHz to 1 kHz, SNR in imaging tissue has dropped by approximately 23 dB (from 30 dB to 6.8 dB), and the three dimensional capabilities are missing from the current system.

3.2. Color imaging

Color imaging using our dual-channel SEE probe was demonstrated by imaging a color print which was positioned on a computer controlled linear stage, allowing two-dimensional scanning of the sample across the probe's focal plane. First, the (monochromatic) reflectivity $r(x(\lambda),y)$ of each sample location encoded by wavelength λ was calculated by dividing each scan (frame) by a reference spectrum, obtained by imaging a white paper. Next, individual spectrally encoded images where captured by scanning the sample in the y-axis, while the field of view was shifted after each capture by a constant amount in the x-axis [25]. After capturing three or more spatially-overlapping frames, the spectral reflectivity at each point was converted to the CIE tristimulus values XYZ using the three CIE standard observer color matching functions $\bar{x}$, $\bar{y}$, and $\bar{z}$ according to [33]:

$$X = \frac{1}{L}\sum_{i=1}^{N}\bar{x}(\lambda_i)\cdot r(\lambda_i), \qquad Y = \frac{1}{L}\sum_{i=1}^{N}\bar{y}(\lambda_i)\cdot r(\lambda_i),$$
$$Z = \frac{1}{L}\sum_{i=1}^{N}\bar{z}(\lambda_i)\cdot r(\lambda_i), \qquad L = \sum_{i}\bar{y}(\lambda_i), \tag{1}$$

where the overlap factor N denotes the number of wavelengths captured for each sample location due to spatial overlap between the frames, and L is the luminance correction factor. The CIE tristimulus values were then converted to sRGB tristimulus values using linear matrix multiplication followed by 2.2 gamma correction [34].

#166904 - $15.00 USD Received 18 Apr 2012; revised 2 Jul 2012; accepted 2 Jul 2012; published 16 Jul 2012

The resulting color images of scans with three spectral data points for each sample locations (N = 3) is shown in Fig. 4(a). While three single wavelengths have been demonstrated sufficient for spectrally encoded color imaging [21,25], here it resulted in noticeable yellow vertical lines in regions where wavelengths bellow 450 nm are missing from the spectrum. Shown in Fig. 4(b) is a CIE-xy 1931 chromaticity diagram with three solid line, dashed line and dotted line triangles enclosing all possible gamut ranges at sample locations marked by the roman numerals I, II and III in the magnified view inset in Fig. 4(a), respectively. Note that the color gamut within the solid triangle which corresponds to sample location I cannot accurately reproduce blue and purple tones within the sRGB range (dotted gray triangle), causing color bias toward yellow which was visible as vertical yellow strikes across the image. Capturing four wavelengths per sample location instead of only three had noticeably improved the color accuracy of the printed sample (Fig. 4(c)). The use of four wavelengths which span noticeably larger color gamut within the three quadrilaterals in Fig. 4(d), allowed almost complete coverage of the sRGB range. As a result, the resulted color image (Fig. 4(c)) had less color banding and better color reproduction across the entire image. A photograph of the printed pattern is shown in Fig. 4(e) for reference.

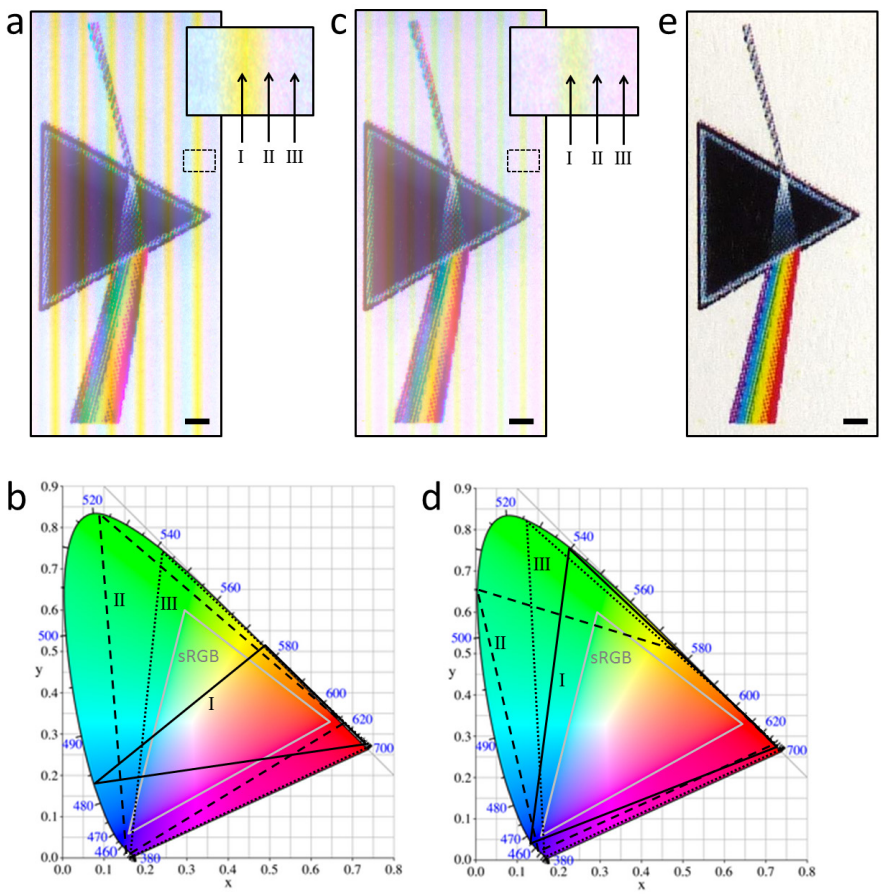

Fig. 4. (a) Color image of a paper print using data from three scans per sample location. The inset shows a magnified region of interest marked by a dashed rectangle. (b) CIE-xy 1931 chromaticity diagram with 3 gamut triangles corresponding to sample locations I, II, III marked in the inset of (a). (c) Same as (a), using data from four scans per sample location. (d) CIE-xy 1931 chromaticity diagram with three gamut quadrilaterals corresponding to sample locations I, II, III marked in the inset of (c). The sRGB gamut range is within the grey triangles in (b) and (d). (e) A digital photograph of the sample. Scale bars represent 1 mm.

#166904 - $15.00 USD Received 18 Apr 2012; revised 2 Jul 2012; accepted 2 Jul 2012; published 16 Jul 2012

4. Discussion

The dual-channel SEE probe presented in this work incorporates recently reported advances in spectrally encoded imaging [21,25,35] into a miniature functional probe, while addressing some of the challenges associated with the construction of previous SEE probes [18]. The first practical challenge was the fabrication of the miniature diffraction grating at the distal end of the probe. The previously reported technique [22] for imprinting the grating pattern on the tip of polished glass rods had numerous difficulties in aligning a large quantity of miniature angled optical substrates as well as in detaching the gratings from their fixture. Using a high power femtosecond laser for cutting small pieces out of large silica gratings allows the use of the highest quality, commercially available bulk gratings which could be cut fully automatically without requiring the use of epoxies, UV-curing glues or chemical processing. A second challenge in the assembly of a dual-channel probe is the co-alignment of the illumination spot and the field of view of the imaging channel. The oval illumination spot in this work was much thicker than the imaging line and thus allowed easy alignment of the relative rotation angle between the fibers, but also resulted in relatively low illumination efficiency; the ratio between the illuminated and the imaged area was only 0.36% and 0.18% for the 0.22 NA and 0.37 NA illumination fibers, respectively. Moreover, from the full bandwidth illuminating each point on the sample, only 1 nm was collected for imaging, resulting in further reduction of the illumination efficiency. A narrower illumination spot could be realized, for example, by using a miniature cylindrical lens at the distal end of the illumination fiber, and higher spectral efficiency could be achieved by using course spectral dispersion in the illumination by further adding a diffraction grating; both techniques could potentially allow several-fold improvement in SNR. Finally, for applications that require full unidirectional probe rotation, a sophisticated optical rotary junction would be required for effective light coupling between the stationary system console and the two rotating fibers (such coupler is commercially available from Princetel Inc., for example).

An important advantage of the dual-channel over the single fiber probe is its ability to control speckle contrast by using incoherent illumination [35]. The reduction in speckle contrast was found to be nearly linear with core diameter, where the 600 μm illumination core had resulted in an essentially negligible speckle noise. While higher core diameters would further reduce speckle, the overall geometrical constrains (diameter, flexibility) would depend strongly on the application. We have found that for our 500 μm diameter imaging channel, a 200 μm illumination core produces tolerable speckle (Fig. 3) without compromising too much the total probe diameter of 700 μm. An alternative technique for speckle reduction would be the use of complex shaped fibers or multiple illumination small core fibers arranged in a more space-efficient configuration.

Another benefit of the system and probe presented in this work is its ability to image color specimens. Using a bright, fiber-coupled white light source, color imaging is possible by additional lateral scanning of the probe in the direction parallel to the spectrally encoded axis. We have found that four encoding wavelengths per sample location are advantageous over three wavelengths, allowing more accurate color rendition with less artifacts. Moreover, it would be possible to conduct a full, high resolution spectral imaging [25] using slow gradual lateral scanning. Future probes with more efficient illumination and a faster line camera could enable such measurements *in vivo*. A possible implementation of endoscopic spectrally encoded spectral imaging could be realized by using two imaging modes: one for real-time monochromatic imaging for in-body navigation, and a second, slow and linear probe motion for acquiring high spectral or color fidelity.

Future development work toward animal studies with our dual-channel SEE system include protective packaging of the probe optics within a flexible sheath, incorporating a dedicated rotational scanning system, and developing an automated color reproduction algorithms for recovering color and spectral information from continuously acquired spectrally encoded frames.

#166904 - $15.00 USD Received 18 Apr 2012; revised 2 Jul 2012; accepted 2 Jul 2012; published 16 Jul 2012

5. Conclusion

A dual-channel SEE system and probe comprised of separated spatially incoherent illumination channel and spectrally encoded imaging channel improves various important imaging parameters compared to previous SEE systems by allowing non-confocal, incoherent imaging. Additionally, by using a larger imaging channel, a higher groove density grating, broader spectrum and shorter wavelength, the presented SEE system brings several-fold improvement in the number of lateral resolvable points, as well as color imaging with low chromatic distortions. The high image quality, color rendition, and straight-forward probe fabrication and assembly may allow SEE to better perform clinical diagnostics tasks which require the use of ultra-miniature flexible endoscopes.

Acknowledgments

The study was funded in part by the Israel Science Foundation grant (716/09) and by the European Research Council starting grant (239986). This work was also supported in part by the Lorry I. Lokey Interdisciplinary Center for Life Sciences and Engineering.